Stabilizing Terahertz MIMO Channel Capacity with Controlled Diffuse Reflections

Suresh Singh
Department of Computer Science
Portland State University
Portland, OR 97207
Email: singh@cs.pdx.edu

Ha Tran
Department of ECE
Portland State University
Portland, OR 97207
Email: thanh4@pdx.edu

Thanh Le
Department of ECE
Portland State University
Portland, OR 97207
Email: tranha@pdx.edu

***Abstract*—Communication at the terahertz band is increasingly seen as vital for future short-range very high datarate channels. However, these channels suffer from significant environmental impairments and, as a result, providing coverage in indoor settings requires the use of directional line of sight (LoS) paths to visible users and reflected paths, using smooth metal reflectors, for users in the shadow of an obstruction. Previous work has shown that these types of reflected paths display similar characteristics to LoS paths and we call them R-LoS (reflected LoS).**

MIMO for LoS and R-LoS channels is feasible at terahertz frequencies and delivers very high capacity at some distances. Unfortunately, channel capacity varies greatly with small changes in distance (the channel matrix fluctuates between full rank and rank 1) which is undesirable for communication systems. In this paper, we utilize *diffusive* reflectors to create multiple reflections such that the MIMO channel capacity for R-LoS is better behaved.

We conduct experiments at 410 GHz for reflections from different artificially created diffuse surfaces. We use measurements to estimate channel capacity for 2x2 MIMO when the only path is the diffuse reflected one. We show that by creating multiple controlled reflections, it is possible to achieve relatively stable capacity up to 13 - 16 bits/sec/Hz at varying distances. We also analyze the phase of the received signals and the beam profile in detail. Overall, our results indicate that by utilizing artificially created reflections, we can maintain a stable MIMO channel at high capacity.

***Index Terms*—Terahertz, channel model, reflection**

I. Introduction

Providing indoor coverage for terahertz cells will require extensive use of reflectors to cover areas that lie in shadows, Figure 1. However, given the severe attenuation suffered by these signals with absorption in the atmosphere [1] and by many common building materials, the reflectors need to be made of materials (such as metal) that minimally alter the signal[1]. In previous work, we developed measurement-based channel models for LoS [2] and reflected signals [3]. As we showed, when reflected from smooth metal plates, the channel models are similar to the LoS model. Additionally, the directional beam produced by the antennas retains its shape even after one reflection from metal. Figure 2 plots the beam cross-section for 410 GHz when using the measurement setup described in section IV. The antenna gain is 25dB. As the figure shows, the LoS transmission and the reflected signal have an almost identical beam cross-section. Therefore, we call the reflected path created by smooth metal surfaces a R-LoS path.

MIMO is a feasible option in LoS (and R-LoS) channels at mmWave and terahertz frequencies [4], [5], which promises to provide significant capacity in terahertz cells. However, as these and other authors have noted, the capacity oscillates with increasing transmitter to receiver distance. Indeed, in a previous paper [6] we experimentally verified this behavior for a 2x2 terahertz LoS MIMO system. We observed variation in channel capacity with distance, with maximum capacity being obtained at distance d when the inter antenna spacing s satisfies Eqn. 3. Between these optimal distances, the capacity sharply reduces [5]. This extreme sensitivity of capacity to small distances makes the communication link unstable (as higher layer protocols attempt to invoke rate adaptation). It is preferable if the link's capacity is stable for longer distances even at the expense of reducing the maximum capacity.

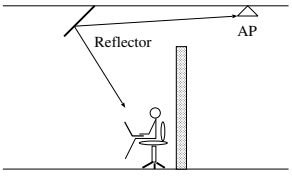

Fig. 1. Use of reflectors for coverage: R-LoS path.

Recently there have been studies on the use of LoS MIMO at mmWave frequencies [4], [7], [8]. Similar to us, these and other authors have noted that at certain distances the channel matrix is full rank thus giving the maximum capacity. However, that changes with increase in distance, as we observed. To mitigate this problem, one suggestion is to use non-uniform arrays to ensure a > 1 rank channel matrix [9] for most distances (by selectively using subsets of array elements) while others have suggested rotating the arrays to maintain maximum rank [10]. Applying these solutions to R-LoS paths is possible but they are fairly complex and require real-time adjustments

This work was funded by the NSF under grant CNS-1910655.

All our data and code is available at: http://web.cecs.pdx.edu/ singh/projects/thzmimo/Home.html

[1]Reflections from metal does not affect the polarization whereas reflections from dielectric or non-metallic surfaces polarizes the wave.

to the antenna arrays (either in the selection of array elements to use or in physically changing the orientation).

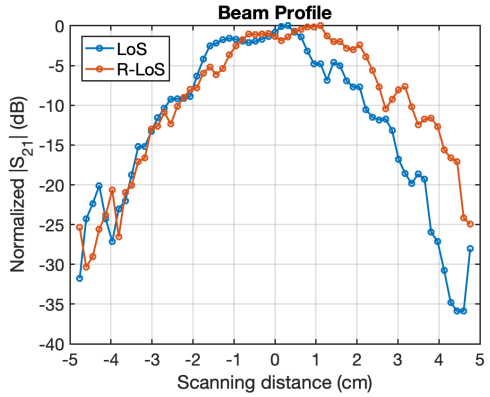

Fig. 2. Beam profile of LoS and R-LoS cases (distance is 20.32 cm).

Our approach for the R-LoS case exploits the use of passive reflectors to maintain a high rank channel matrix. Specifically, by fabricating reflectors that provide multiple paths of slightly varying lengths, we show that a high rank channel matrix can be maintained over variable transmitter to receiver distances. We illustrate this behavior by experimentally measuring the capacity of a 2x2 MIMO system with diffusive reflections and comparing it against a R-LoS case when there is one reflection from a smooth metal surface. *Our main results show that (a) our approach does indeed stabilize capacity and (b) in some cases, it provides a higher capacity (16-17 bps/Hz, Fig. 18) than when we do not use diffuse reflectors (14-16 bps/Hz, Fig. 8).* The remainder of the paper is organized as follows:

- In the next section we describe our system model in more detail,
- Subsequently in section III we discuss related work in the context of LoS MIMO capacity and the use of reflective surfaces,
- In section IV we describe the testbed used and experimentally study the channel characteristics of the R-LoS case with one reflection,
- The design of four different reflectors is provided in section V where we also examine the phase and beam shape of the reflection produced by one of the four surfaces,
- Section VI presents our measurement results for 410 GHz and we examine the variation of capacity with distance,
- Finally we conclude in section VII.

II. System Model

As has been noted previously [4] LoS MIMO channels are possible at mmWave and higher terahertz frequencies because the planar wavefront model of propagation between transmit and receive arrays does not hold true when the distances being considered are small enough that the curvature of the wavefront is no longer negligible relative to the wavelength. Thus, the channel response for the LoS and R-LoS channels can be written as a $n \times n$ matrix,

$$\mathcal{H} = \left[e^{-jkd_{ij}}\right] \tag{1}$$

where the Tx and Rx are assumed to have n antennas each, d_{ij} is the distance between the ith transmit antenna and the jth receive antenna, and $k = 2\pi/\lambda$. The channel capacity [5] is then simply,

$$\mathcal{C} = \log_2\left(\det\left(\mathcal{I} + \frac{\rho}{n}\mathcal{H}\mathcal{H}^\dagger\right)\right) \text{ bps/Hz} \tag{2}$$

Note that this formulation ignores attenuation effects due to absorption in the atmosphere and at the reflective surface and other impairments [2]. However, since none of these effect the key idea behind LoS MIMO, we are leaving them out of the discussion for now. All these effects do manifest themselves in our measurements as we discuss in later sections.

The capacity Eq. 2 is maximized when $\mathcal{H}\mathcal{H}^\dagger = n\mathcal{I}_n$ (where $\mathcal{I}_n$ is the identity matrix) and ρ is the SNR. It is easy to then derive a relationship between inter-antenna spacing s and Tx-Rx distance d,

$$s^2 = (2p+1)\frac{d\lambda}{2}, \text{ where } p = 0, 1, 2, \cdots \tag{3}$$

Fig. 3 plots the capacity formula for 2x2 R-LoS MIMO as a function of d and we observe the maximum values attained when the above relationship is satisfied. As we see, capacity varies by a factor of 2x over short variations in distance.

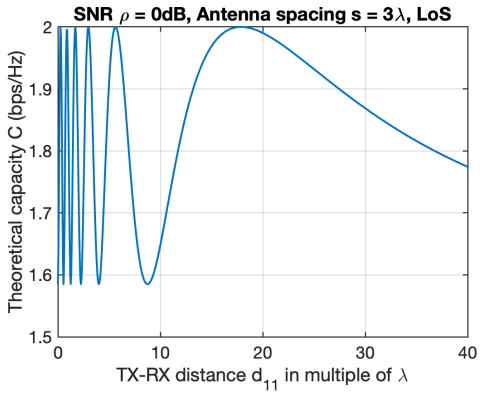

Fig. 3. Theoretical capacity for R-LoS 2x2 MIMO (45^o angle of incidence).

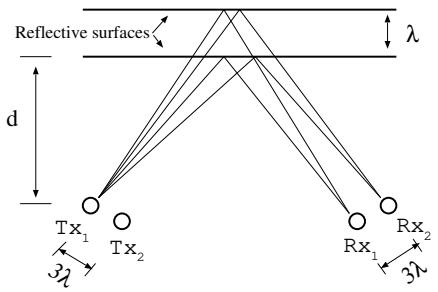

Fig. 4. Example of two reflective paths.

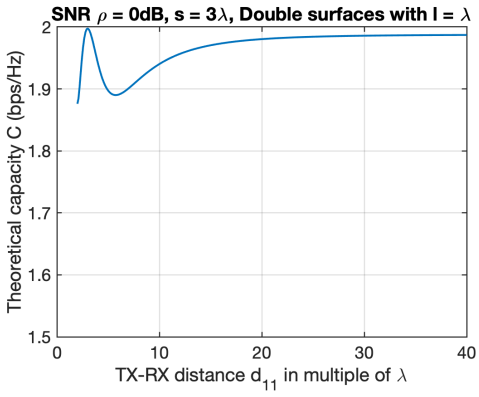

Fig. 5. Theoretical capacity as a function of TX-RX distance for R-LoS 2x2 MIMO with the addition of 2 reflective surfaces.

In this paper, we propose using diffusive reflective surfaces that *produce multiple reflections resulting in varying path lengths*. Assume that there are m_{ij} paths between transmit antenna i and receive antenna j and the path length of each is $d_{ij}^l, 1 \leq l \leq m_{ij}$. We also assume that each path carries a normalized fraction of the signal energy α_{ij}^l. Using the above formulation, we can write the $n \times n$ channel response as,

$$\mathcal{H}_{\text{diffuse}} = \left[\sum_{l=1}^{m_{ij}} \alpha_{ij}^l e^{-jkd_{ij}^l} \right] \tag{4}$$

Note that the above model is a direct extension of the LoS model because the reflections are *controlled*. Also, unlike a standard Rician formulation or scattering formulation [11], we are able to account for each reflected path which allows us to specify the phase accurately.

As an example, consider the case of two reflective paths in Fig. 4. Assuming both paths have the same SNR, we obtain a capacity curve as shown in Fig. 5. Comparing this with Fig. 3 we see that adding an additional reflector does stabilize capacity.

In this paper, we experiment with four different reflective surfaces built using metal and analyze how well they can stabilize the capacity.

III. Literature Review

In order to stabilize the capacity of R-LoS MIMO, we propose using reflections such that the channel matrix remains full rank or as close to it as possible. We note however that there has been prior work on the use of reflectors in mmWave and even in terahertz systems and we summarize those results below.

Previous work has studied two types of reflectors – *passive* and active. Active reflectors are called *re-configurable intelligent surfaces* (RISs). These surfaces can be electronically configured to phase shift the incident signals to achieve good channel conditions at the receiver. Thus, [12] presents a closed-form expression that allows phase-shifting optimization of each reflection unit of the RIS. This work is extended in [13] in order to include the effect of turbulence and stochastic beam misalignment. Meanwhile, in [14], the authors used exact statistical characterizations of end-to-end signal-to-noise ratio to optimize the phase shift at RIS elements. Furthermore, in [15], the authors utilized RIS to enhance self-interference cancellation for in-band full-duplex communication systems.

The use of *passive reflectors* has been explored in the context of improving coverage in 5G mmWave cells for urban scenarios. For instance, [16] develops a simple NLoS channel model for reflections from building tops to users on the ground. [17] proposes an optimization framework for the joint placement of gNBs and reflectors in urban geometries in order to improve coverage. [18] considers the reflector placement problem in indoor scenarios where the LoS path of a mmWave AP is obstructed. For indoor terahertz cells, [19] proposes using dielectric mirrors placed on all the walls to provide coverage in rooms.

Finally, there has been a great deal of measurement-based work on terahertz reflections from different surfaces. For instance, there has been work done on terahertz reflections from vehicles [20], indoor materials including drywall, clear glass as well as stratified building materials [21], [22], and different metals [22].

The work we present in this paper clearly differs from work done on characterizing reflections from different materials (though the reflection coefficients obtained there can be used in our models). Our work also differs from the use of RISs for beamforming since our goal is creating multiple reflective paths rather than beamforming. Finally, while previous work on the use of passive reflectors is not related to our goal, we show that using multiple passive reflectors can ensure that the channel capacity is stable over varying distances.

IV. Measurement Setup

A Rohde & Schwartz Vector Network Analyzer (VNA) and Virginia Diode, Inc. (VDI) frequency extender modules are utilized to collect elements of the transfer matrix H_{ij}. In this paper specifically, the WR2.2 band extender module is used to generate signals from 325 GHz to 500 GHz. In order to eliminate mismatched effects from cable and connections, the system is calibrated before all the measurements using Thru-Reflect-Line (TRL) standards. After the calibration process, the measurement reference plane is moved to the waveguide opening. Other important VNA settings are mentioned in Table I. The setup employs a pair of 25dB gain, 1.68 cm long antennas to transmit and receive signals. Depending on the experiments, other specifications of the setup consisting of incident angles, direct or reflective measurements, TX-RX distance, antenna spacing, etc. are described separately for each setup. Note that in this paper, all distances are measured from one antenna's aperture to the other's.

Note that the VNA collects transmission coefficients S_{21} used as elements of the transfer matrix. Plots of S_{21} in this paper represent the ratio of received power over transmitted power. The actual power received at the RX antennas can be calculated by multiplying the output power from Table I.

TABLE I
VNA SETTING (WR2.2 FREQUENCY BAND)

Output power	5 dBm
Frequency range	325 - 500 GHz
Frequency step	0.1 GHz
IF Bandwidth	1 kHz
Averaging	10
Calibration method	Thru-Reflect-Line

A. Measurement of of a 2x2 R-LoS MIMO system

The limitation of these types of channels, illustrated in Fig. 3, is demonstrated experimentally using our testbed. In this set of experiments, the optimal distance d_{opt} between the transmitter and receiver is picked as 21.55 cm ($6 * \sqrt{2}$ in) and antenna spacing s_{opt} is calculated for the center frequency of 410 GHz to be 0.89 cm using Eq. 3. We consider two sets of measurements. In the first, we keep the distance d fixed at 21.55 cm and vary the inter-antenna spacing s. In the second, we fix $s = 0.89$ cm and vary d. For this second case, we plot the estimated capacity directly using Eq. 3. An angle of incidence of 45^o is used for all measurements.

We label the two transmit antennas ax Tx1 and Tx2 and the receive antennas as Rx1 and Rx2. Fig. 6 and Fig. 7 show the phase difference and the summation of received signals at the receiver Rx1 for different inter-antenna spacing. The phase differences of the two signals (from Tx1 and Tx2) arriving at Rx1 vary over $\sim 2\pi$. If we sum the signals at Rx1, we get the behavior illustrated in Fig. 7. In Fig. 8 we plot the estimated capacity as a function of distance. For this, we empirically measured the $\mathcal{H}$ matrices and then used Eq. 2. As all of these plots show, the MIMO channel at 410GHz does exhibit behavior consistent with the theory in Section 2.

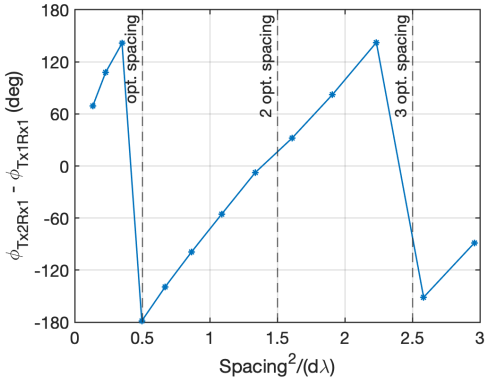

Fig. 6. Phase difference of received signals at Rx1 from Tx1 and Tx2 illustrating that signals go in and out of phase.

V. CREATING MULTIPLE REFLECTIONS

We experimented with different methods to create multiple reflected paths between the transmitter and receiver. The goal is to ensure that the phase of the signals arriving at receive antennas are decorrelated. Given the small wavelength of 410 GHz, this implies that the reflective surfaces need to have

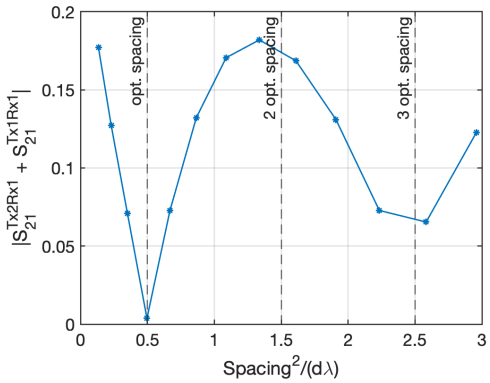

Fig. 7. Summation of receiving signals at RX1 for the R-LoS case showing minimal magnitude at an odd number of optimal spacing and maximum at twice optimal spacing.

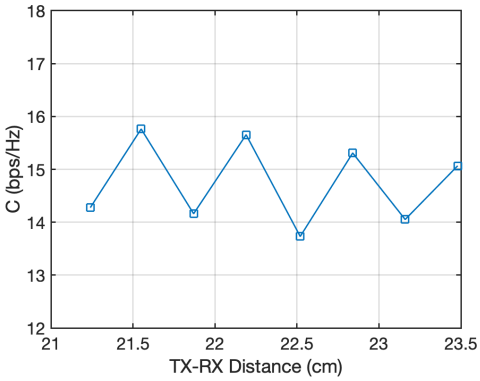

Fig. 8. Capacity of of R-LoS with smooth aluminum plate reflector shows alternate peaks and dips over TX-RX distances.

deformities of the order of the wavelength. Simultaneously, we need to ensure that the reflective material does not attenuate the signal significantly. With these requirements in mind, we studied the following four reflective surfaces:

- **Pins-3R:** We first consider the structure consisting of an aluminum plate with 3 rows of short pins in front as shown in Fig. 9. Each row is 5 mm away and the pins with diameter of 1.5 mm are placed at 5 mm spacing
- **Pins-5R:** Similar to Pins-3R structure but denser with 5 rows of pins. Row separation is 2.5 mm and pin spacing is 5 mm (Fig. 9).
- **Blades-H**: Wavy-surface metal blades are aligned horizontally (Fig. 16)
- **Blades-V**: Similar to Blades-H structure but the wavy-surface metal blades are aligned vertically.

All of these surfaces scatter the incident signal but to evaluate if they meet the criteria of multiple decorrelated paths, we repeated the analysis of phase and received signal strength. In the next section, we provide this analysis for Pins-3R structure – the other surfaces exhibit similar properties.

A. Phase Analysis of Pins-3R Structure

Using the same methodology as in section IV-A we keep the distance d between the transmitter and receiver fixed but vary the inter-antenna spacing s. The phase difference and magnitude summation of the received signals are plotted in Fig. 10 and Fig. 11 respectively. Comparing Fig. 10 with Fig. 6 we note that the phase difference shows more variability than the case of a single reflection. Likewise, when we compare the total received magnitude Fig. 11 with Fig. 7 we note that the magnitude does not have minima or maxima with Pins-3R. Of course, we note that the total amplitude is lower when using these diffusive surfaces. This is to be expected since the signal shows greater angular scattering and is not captured by the receive antennas.

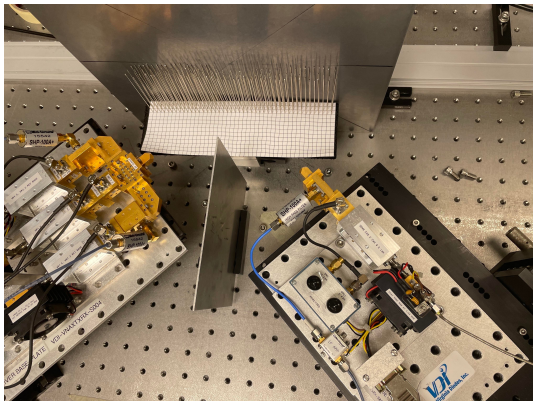

Fig. 9. Proposed structure with thin metal pins at 45^o angle of incident. There are 2 configurations: Pins-3R consists of 3 rows of pins at 5 mm spacing, 5 mm row separation; and Pins-5R with 5 rows, 5 mm pins spacing, 2.5 mm row separation.

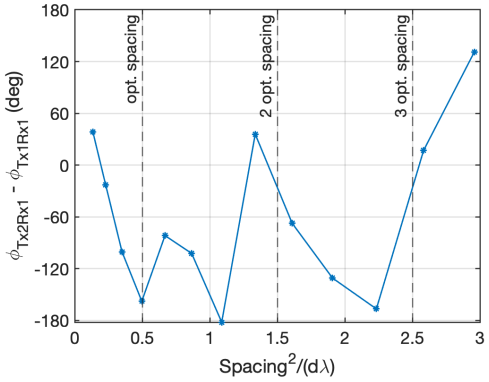

Fig. 10. Phase different of received signals of proposed structure Pins-3R.

We next looked at the time domain response of the system which is obtained from the frequency domain signals from 325 GHz to 500 GHz using MATLAB's Inverse Fast Fourier Transform. The 0.1 GHz frequency step allows a time domain resolution of approximately 5.71 ps. Fig. 12 shows a dominant component for the case when there is a single dominant reflection (for the case from section IV-A). The response for

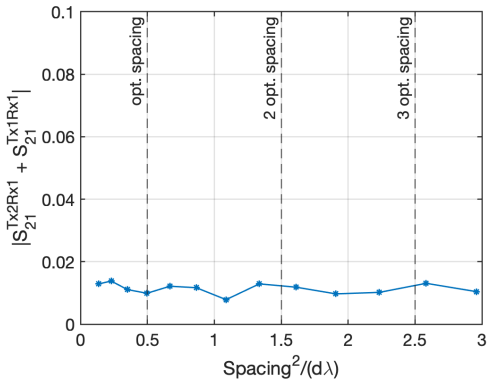

Fig. 11. Sum of received signals of proposed structure Pins-3R.

surface Pins-3R is shown in Fig. 13 where we clearly see the same dominant component and many additional reflections with different delays. The reason that we still have the large main component is that we use an aluminum plate behind the pins.

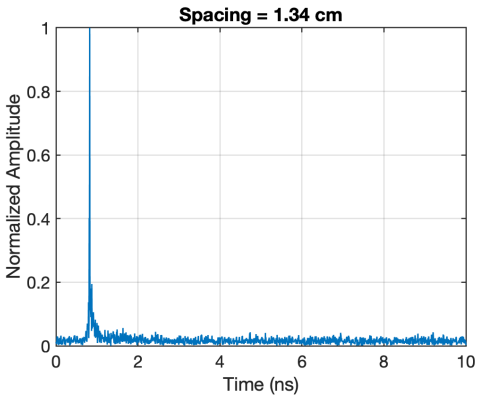

Fig. 12. IFFT of the measurement using only an aluminum plate as the reflector with one dominant component from the main reflection path.

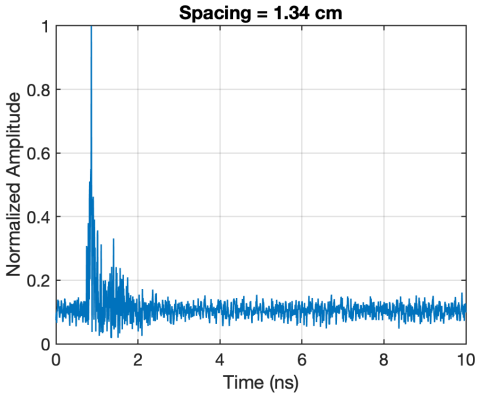

Fig. 13. IFFT of proposed structure showing the same dominant component as in Fig. 12 and plenty of multipath components with different delays.

We also examined the beam profile after the signal undergoes reflection. To conduct this measurement, we block

the beam using a metal plate in increments and record the received signal. The beam profile for the LoS/R-LoS case is shown in Fig. 2 while Fig. 14 shows the profile for reflections from Pins-3R. We note that the beam changes from being highly directional to flatter. This is due to scattering and it also explains why the received signal magnitude is smaller for Pins-3R.

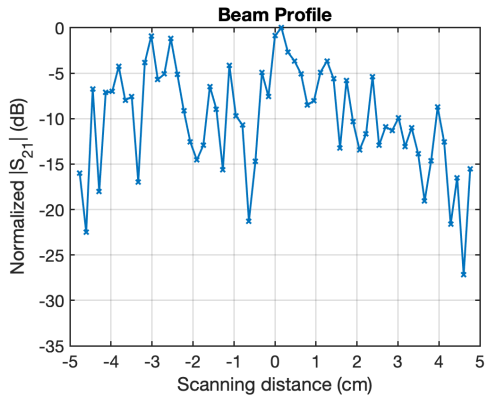

Fig. 14. A flatter beam profile is obtained with structure Pins-3R.

From the above analysis, we can conclude that adding the pins provides multiple reflections as we wanted. In the next section, we evaluate the capacity of the four different reflective surfaces.

VI. Capacity Analysis for Different Structures

To analyze the capacity of different structures, we conduct 2x2 MIMO measurements for varying distances. The MIMO measurement diagram is shown in Fig. 15 and is kept the same for all the measurements. Using a distance of d = 21.55 cm as in section IV-A for center frequency of 410 GHz we obtain inter-antenna spacing s_{opt} = 0.89 cm. We conducted all measurements with this value of inter-antenna spacing and varied the distance d between 21 and 23.5cm. The angle of incidence is kept at 45^o for all measurements. *We restricted our measurements to this small range of distances because it is sufficient to show capacity fluctuation (Fig. 8) and because the equipment used has limited power.*

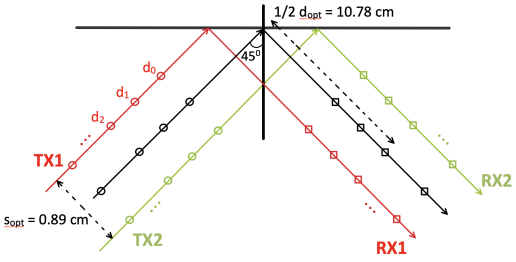

Fig. 15. Diagram of linear 2-by-2 MIMO measurement with reflection surface and multipath structures.

The capacity of the channel is calculated using Eq. 2. In order to evaluate channel capacity under the same SNR

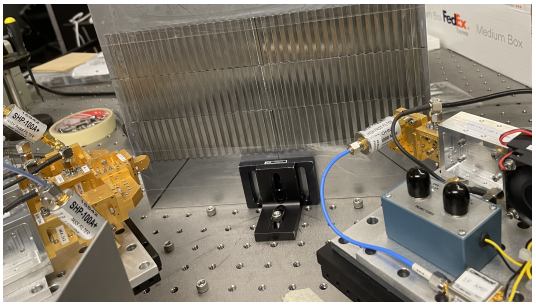

Fig. 16. Measurement setup with wavy metal blades aligned horizontally (Blades-H) at 45^o angle of incident. Note: Blades-V structure is similar but with vertically-aligned blades.

level at 60dB, the measured transfer matrix is required to be normalized. In this paper, the Frobenius normalization is used:

$$\sum_{i=1}^{n_t}\sum_{j=1}^{n_r}|h_{ij}|^2 = n_r n_t \tag{5}$$

where h_{ij} are the measured elements of the transfer matrix, n_t and n_r are the number of transmitter and receiver respectively.

A. Results

Recall from Fig. 8 that the capacity for R-LoS with a single reflection shows multiple peaks and dips alternately over varying distances d. The capacity of reflectors with metal pins (Pins-3R and Pins-5R) are plotted in Fig. 17. As we can see in the figures, Pins-3R gives a great improvement in terms of flat capacity response over various distances but the magnitude is quite low. On the other hand, the Pins-5R structure provides higher capacity but the response is not as flat as in the case of structure Pins-3R.

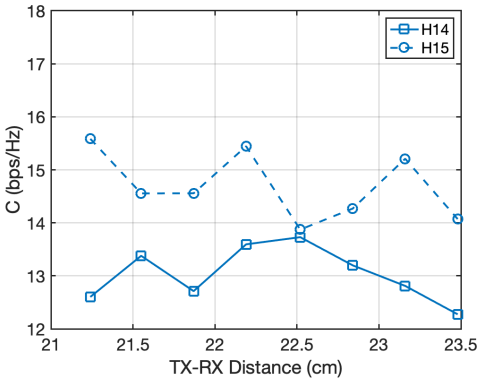

Fig. 17. Capacity of the structures using metal pins: Pins-3R with 3 rows of pins (solid) and Pins-5R with 5 rows of pins (dash). Pins-3R shows a flat response versus TX-RX distances but the magnitude is reduced. Pins-5R response is improved in magnitude but not as flat at Pins-3R case.

Fig. 18 plots the capacity versus TX-RX distance of the reflectors with the wavy metal blades aligned horizontally (Blades-H) and vertically (Blades-V). As illustrated in the figure, the horizontal alignment case (solid line) provides a flat response but with low magnitude. With vertical alignment, a

huge improvement in magnitude is obtained but the response shows a pair of peaks and valleys with varying distance.

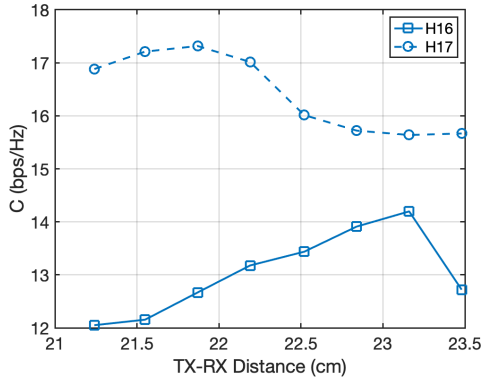

Fig. 18. Capacity of the structures using wavy metal blades: Blades-H with horizontal blades (solid) and Blades-V with vertical blades (dash). Blades-V shows an improvement in both magnitude and consistency over TX-RX distance compared to Blades-H.

Based on the experiments, we can conclude that we can maintain a well conditioned channel matrix for variable distances for MIMO by using reflectors that introduce multiple reflective paths. The channel capacity shows greater stability across varying transmitter to receiver distances. However, we also observe that the four reflective surfaces studied have shortcomings including lower SNR (Pins-3R, Pins-5R) and not a perfectly flat capacity as in the ideal case illustrated in Fig. 5. We believe that other types of reflective surfaces may be able to come closer to achieving this goal.

VII. Conclusion

MIMO is an attractive design choice for ensuring high capacity LoS and R-LoS terahertz channels for future communication systems. However, the capacity of these channels oscillates with distance due to the channel response matrix varying between full rank and single rank. In order to overcome this problem, we propose a solution that is effective for *indoor* environments. Specifically, we propose using diffusive wall-mounted reflectors that scatter the signal in a controlled manner. The goal is to ensure multiple time-delayed paths to the receiver that are minimally attenuated.

We provided measurements of a R-LoS MIMO case that illustrates the problem. We then developed four different types of reflectors and conducted the same measurements again. Our results show that we can indeed maintain a more stable capacity with varying distance. However, we believe that the design of the reflectors can be improved to provide better signal quality at the receiver. This is part of future work.

References

[1] John Federici and Lothat Moeller. Review of terahertz and subterahertz wireless communications. *Journal of Applied Physics*, 107, 2010.

[2] Ha Tran, Thanh Le, and Suresh Singh. Effect of Standing Wave on Terahertz Channel Model. In *2021 IEEE International Conference on Communications Workshops (ICC Workshops)*, pages 1–6, 2021.

[3] Ha Tran, Thanh Le, and Suresh Singh. Reflection Channel Model for Terahertz Communications. In *2022 IEEE International Conference on Communications*, June 2022.

[4] Angel Lozano. Old theory up to new tricks. *IEEE ComSoc Technology News*, August 2021.

[5] Mario H. Castañeda Garcia, Marcin Iwanow, and Richard A. Stirling-Gallacher. Los mimo design based on multiple optimum antenna separations. In *2018 IEEE 88th Vehicular Technology Conference (VTC-Fall)*, pages 1–5, 2018.

[6] Suresh Singh, Thanh Le, and Ha Tran. Measurement of 2x2 LoS Terahertz MIMO Channel. In *2020 IEEE Wireless Communications and Networking Conference (WCNC)*, pages 1–5, May 2020.

[7] Heedong Do, Namyoon Lee, and Angel Lozano. Reconfigurable ulas for line-of-sight mimo transmission. *IEEE Transactions on Wireless Communications*, 20(5):2933–2947, 2021.

[8] P. Raviteja and U. Madhow. Spatially oversampled demultiplexing in mmwave los mimo. In *2018 IEEE 19th International Workshop on Signal Processing Advances in Wireless Communications (SPAWC)*, pages 1–5, 2018.

[9] G. D. Surabhi and A. Chockalingam. Compact antenna spacing in mmwave mimo systems random phase precoding. In *IEEE 86th Vehicular Technology Conference (VTC-Fall)*, 24-27 September 2017.

[10] Heedong Do, Sungmin Cho, Jeonghun Park, Ho-Jin Song, Namyoon Lee, and Angel Lozano. Terahertz line-of-sight mimo communication: Theory and practical challenges. *IEEE Communications Magazine*, 59(3):104–109, 2021.

[11] Z. Xu, X. Dong, and J. Bornemann. A statistical model for the mimo channel with rough reflection surfaces in the thz band. (8):25–34, 2016.

[12] Alexandros-Apostolos A. Boulogeorgos and Angeliki Alexiou. Coverage Analysis of Reconfigurable Intelligent Surface Assisted THz Wireless Systems. *IEEE Open Journal of Vehicular Technology*, 2:94–110, 2021.

[13] Alexandros-Apostolos A. Boulogeorgos, Nestor Chatzidiamantis, Harilaos G. Sandalidis, Angeliki Alexiou, and Marco Di Renzo. Performance Analysis of Multi-Reconfigurable Intelligent Surface-Empowered THz Wireless Systems, February 2022. Comment: 7 pages, 3 figures, IEEE ICC 2022. arXiv admin note: substantial text overlap with arXiv:2106.15082.

[14] Hongyang Du, Jiayi Zhang, Ke Guan, Dusit Niyato, Huiying Jiao, Zhiqin Wang, and Thomas Kürner. Performance and Optimization of Reconfigurable Intelligent Surface Aided THz Communications. *IEEE Transactions on Communications*, 70(5):3575–3593, May 2022.

[15] Simon Tewes, Markus Heinrichs, Paul Staat, Rainer Kronberger, and Aydin Sezgin. Full-Duplex meets Reconfigurable Surfaces: RIS-assisted SIC for Full-Duplex Radios. In *ICC 2022 - IEEE International Conference on Communications*, pages 1106–1111, May 2022. Comment: 6 pages, 9 figures, Accepted for publication in IEEE International Conference on Communications (ICC) 2022.

[16] Zhangyou Peng, Linxiao Li, Miao Wang, Zhonghao Zhang, Qi Liu, Yang Liu, and Ruoran Liu. An effective coverage scheme with passive-reflectors for urban millimeter-wave communication. *IEEE Antennas and Wireless Propagation Letters*, 15:398–401, 2016.

[17] Chethan Kumar Anjinappa, Fatih Erden, and Ismail Güvenç. Base station and passive reflectors placement for urban mmwave networks. *IEEE Transactions on Vehicular Technology*, 70(4):3525–3539, 2021.

[18] Ang Deng, Yuchen Liu, and Douglas M. Blough. Maximizing coverage for mmwave wlans with dedicated reflectors. In *ICC 2021 - IEEE International Conference on Communications*, pages 1–6, 2021.

[19] Michael Taynnan Barros, Robert Mullins, and Sasitharan Balasubramaniam. Integrated terahertz communication with reflectors for 5g small-cell networks. *IEEE Transactions on Vehicular Technology*, 66(7):5647–5657, 2017.

[20] Johannes M. Eckhardt, Vitaly Petrov, Dmitri Moltchanov, Yevgeni Koucheryavy, and Thomas Kürner. Channel Measurements and Modeling for Low-Terahertz Band Vehicular Communications. *IEEE Journal on Selected Areas in Communications*, 39(6):1590–1603, June 2021.

[21] Yunchou Xing, Ojas Kanhere, Shihao Ju, and Theodore S. Rappaport. Indoor Wireless Channel Properties at Millimeter Wave and Sub-Terahertz Frequencies. In *2019 IEEE Global Communications Conference (GLOBECOM)*, pages 1–6, December 2019.

[22] Jianjun Ma, Rabi Shrestha, Lothar Moeller, and Daniel M. Mittleman. Invited Article: Channel performance for indoor and outdoor terahertz wireless links. *APL Photonics*, 3(5):051601, May 2018.